MEMORANDUM

GASEOUS HYDROGEN BURNED IN A SIMULATED AFTERBURNER USING SEVERAL LOW-DRAG FUEL-INJECTOR-FLAMEHOLDER TYPES

By William R. Kerslake

Lewis Research Center
Cleveland, Ohio

NATIONAL AERONAUTICS AND SPACE ADMINISTRATION

WASHINGTON

June 1959

NATIONAL AERONAUTICS AND SPACE ADMINISTRATION

MEMORANDUM 2-24-59E

GASEOUS HYDROGEN BURNED IN A SIMULATED AFTERBURNER USING SEVERAL LOW-DRAG FUEL-INJECTOR-FLAMEHOLDER TYPES *

By William R. Kerslake

SUMMARY

Combustion efficiency and burner pressure loss were measured for seven fuel-injector-flameholder configurations. The configurations were tested in a connected-pipe burner 13 inches long with a cross section equal to a 35° sector of a full 28-inch-diameter afterburner. Combustion efficiencies varied from 92 to 85 percent for the better configurations. Flameholder pressure losses were 1 to 2 percent of the burner pressure loss for the best configurations. The inlet temperature of 1660° R was achieved by a hydrogen-fueled preheater located directly upstream of the afterburner. The inlet pressure was about 1/3 atmosphere, and the velocity was 400 or 500 feet per second.

INTRODUCTION

The use of hydrogen fuel for high-altitude jet engines has been proposed in reference 1. Its use offers the advantages of a high heating value (51,000 Btu/lb), as well as a fuel with a large heat-sink capacity, useful for high-flight-speed cooling requirements. Because of the fast flame speed and the great reactivity of hydrogen, it can be expected that a high combustion efficiency can be realized even at many operating conditions where a hydrocarbon fuel could not burn. The drawbacks of using hydrogen fuel are: (1) the low density as a liquid, necessitating large fuel tanks, and (2) the difficult handling problems associated with a cryogenic fluid.

Gaseous hydrogen as an afterburner fuel has been tested in references 2 and 3 using spray-bar fuel injectors. These injectors are similar to those used in the ramjet combustors of references 4 and 5. The connected-pipe combustion efficiency data of reference 2 are over 90 percent for broad bands of fuel-air ratios, but the data were taken at

*Title, Unclassified.

a moderately high combustor pressure of 1/2 to 1 atmosphere. The full-scale data of reference 3 report sharply falling combustion efficiencies, probably due to the much lower combustor pressure of 1/6 to 1/2 atmosphere.

The work described herein was undertaken in an attempt to find an efficient and more stable gaseous-hydrogen fuel-injector-flameholder for low-pressure afterburner use. The specific goals were (1) a low-drag, durable, fuel-injector-flameholder and (2) high combustion efficiencies at 1/3 atmosphere over a wide band of fuel-air ratios.

Combustion efficiencies and burner pressure losses were determined at afterburner-inlet conditions of an advanced turbojet engine (flight Mach number, 4.0 and compressor pressure ratio, 2.3), pressures of 10 to 12 inches of mercury absolute, velocities of 400 and 500 feet per second, and a temperature of 1200° F. The inlet air temperature was achieved by a hydrogen-fueled preheater located immediately upstream of the afterburner test section. Additional tests consisted of (1) measuring the blowout velocity at ambient air temperatures, and (2) intentionally pulsing the airflow to impose more severe conditions on the better fuel-injector-flameholder configurations.

APPARATUS

Connected-Pipe Test Facility

A schematic drawing of the airflow is shown in figure 1. Air was supplied at 40 pounds per square inch gage and 540° R (80° F). Flow was metered by a variable-area calibrated orifice and passed through a throttling valve into a plenum chamber. From the plenum chamber it was ducted in a 12-inch-diameter pipe to the preheater combustor section. The preheater fed directly into the afterburner combustor section.

Gaseous-hydrogen fuel was supplied from a multicylinder trailer to both the preheater and afterburner fuel systems. Each fuel system contained a throttling valve and a calibrated critical-flow metering orifice. The valving arrangement permitted use of either fuel line separately or both simultaneously.

Air-atomized quench water, metered by calibrated rotameters, was sprayed into the gases at the afterburner exit. The equilibrium mixture temperature was measured by two thermocouple rakes at the end of a 15-foot-long heat balance or calorimeter section. The gases then flowed through a throttling valve to the laboratory altitude exhaust system. The calorimeter wall temperature was measured by skin thermocouples to permit calculation of heat losses from the calorimeter. Windows at either end of the rig permitted observation of the afterburner.

Afterburner Section

Details of the 35° annular sector combustor are presented in figure 2. The combustor simulated a section of a 28-inch-diameter afterburner with a $9\frac{1}{4}$-inch-diameter centerbody. Fuel injectors were inserted through a flanged hole in the 28-inch-diameter curved wall. The combustion distance from the fuel injectors to the quench-water spray was 13 inches. The burner walls were cooled by forced-air convection. Total-pressure rakes, wall static-pressure taps, and a thermocouple rake were located as shown in figure 2. The total-pressure rakes, installed late in the program, were used only with the last fuel-injector-flameholder configuration.

A microphone-type pressure pickup was mounted on an "infinite tube" arrangement to measure static-pressure fluctuations at the afterburner wall. The "infinite tube" probe, similar to that used in reference 6, was positioned at various intervals along the afterburner length to locate a pressure antinode.

Preheater Section

The preheater section was formed by an upstream continuation of the afterburner walls. The preheater fuel injectors, located 19 inches upstream of the afterburner injectors, are described in reference 7 as configuration J, four shrouded spray bars. Air entered the preheater through an orifice-type flow restriction 20 inches upstream of the fuel injectors. The preheater fuel flow was theoretically sufficient to produce a temperature of 1660° R. A sparkplug located on the side wall and downstream of the fuel injectors ignited the preheater.

Fuel-Injector-Flameholder Configuration

Figure 3 presents details of the fuel injectors. Configuration A was chosen to start the program because it had performed well in a turbojet primary-burner application (ref. 8). For afterburner use the restriction ring in the entrance of the swirl can used in reference 6 was removed to reduce the flameholder blockage area. The number and spacing of the swirl cans were based on the assumption that each one would spread the flame about three or four times its outlet area. Reference 8 indicates that this assumption is valid for the size swirl can used and for a burner length of 13 inches.

Configuration B consisted of radially flattened spray bars. The injection holes were equally spaced, but of different sizes to balance fuel flow with cross-sectional area. The plain spray bars were tested

to learn if they would perform well at combustion pressures lower than those of reference 2 (15 to 30 in. Hg abs) but higher than those of reference 3 (5 to 8 in. Hg abs).

Configuration C, shielded spray bars (fig. 3(c)), was an attempt to improve the stability of plain spray bars by applying shielding. The spray bars were the same as configuration B. The shield divergence and hole area were so designed (using theoretical hole flow coefficients and assuming partial heat addition inside the shields) that the gases inside the shield would leave with the same velocity as the secondary air that was accelerated around the shields.

Configuration D, piloted spray bars, consisted of a radial spray bar with a reverse-teardrop cross section. A small U-shaped shield on the leading edge of the bar formed a piloting zone. The shield had holes in the leading edge to admit air. About 17 percent of the fuel was injected upstream into the piloting zone with the bulk of the fuel injected 45° downstream. The 45° angle was chosen as a compromise between requirements for fuel spreading and for recovery of the pressure momentum of the fuel. The main fuel-injection holes were of one size, but of variable radial spacing (in centers of equal areas) to obtain even fuel distribution.

Configuration E, V-gutter injectors, was designed after the best ramjet hydrogen-fueled injector configuration of reference 9. The configuration was built up from two main radial supply tubes as shown in figure 3(e). Each of the radial tubes had eight side-arm V-gutters. A single fuel hole injected fuel into each of these V-gutters at right angles to the airflow. The V-gutter provided a flameholding zone as well as a region to allow the fuel to spread out before being swept down the combustor.

Configuration F is called "Pabst burners" because the design is identical to a fuel injector described in reference 10, a translation by a British scientist named Pabst of experimental work done in Germany at the end of World War II on a hydrogen-fueled Focke-Wulf subsonic ramjet. Sixteen individual conical-shaped fuel-injector elements were separately fed from a branching tube arrangement as shown in figure 3(f). The fuel is injected through a circular slot located near the base of the conical-shaped element. The slot is normal to the airstream, but the fuel is quickly swept downstream because of the low fuel-injection velocity.

Configuration G, shrouded spray bars, was identical to a fuel-injector-flameholder configuration tested in reference 7 at ramjet operation conditions. The configuration consisted of a flattened spray bar inside a U-shaped gutter or shroud as shown in figure 3(g). The shroud contained air admission holes in the leading edge, while the trailing edge was bent to form mixing tabs. As the projected blockage area of

this configuration was much greater than those of the previous configurations, it was anticipated that the drag losses would be higher. It was, nevertheless, tested to see if such a promising ramjet configuration could withstand the high inlet temperatures encountered in an afterburner. Even though the drag losses might be too high for the particular engine considered in this report, it was thought that a future application could tolerate additional drag in exchange for the increased stability and burning range expected of this configuration.

PROCEDURE

Standard Operating Conditions

For all seven fuel-injector-flameholder configurations, combustion efficiency and pressure loss data were taken at two nominal afterburner-inlet conditions: (1) a low velocity, 400 feet per second; pressure, 12 inches of mercury absolute; and temperature, 1660° R, and (2) a high velocity, 500 feet per second; pressure, 10 inches of mercury absolute; and temperature, 1660° R. The conditions simulated two possible inlet flows to an afterburner of an advanced turbojet engine. A run was defined as a series of data points at constant afterburner-inlet conditions with changes in the afterburner fuel flow. At the start of a run the preheater was first turned on alone, and its combustion efficiency was measured by the heat balance. (The thermocouple rake measuring the afterburner-inlet temperatures was only used to set the preheater fuel flow and check the approximate temperature.) By knowing the preheater combustion efficiency and equivalence ratio, a preheater-outlet or afterburner-inlet temperature was calculated. Equivalence ratio was defined as the actual fuel-air ratio divided by the stoichiometric fuel-air ratio, 0.0292. The over-all equivalence ratio is simply the sum of the actual preheater and afterburner fuel-air ratios divided by 0.0292. (The preheater combustion efficiency was assumed to remain constant for the entire run because of the nearly constant operating conditions.) The afterburner-inlet velocity was calculated by the continuity equation using wall static pressure and calculated preheater-outlet temperature. The preheater was located close enough to the afterburner that heat losses were negligible.

Over-All Combustion Efficiency

Combustion was terminated by the quench-water spray, and the total enthalpy rise of the afterburner plus the preheater burner was calculated from a heat balance around the calorimeter. Over-all combustion efficiency was defined as the total measured enthalpy rise divided by the theoretical lower heating value of the fuel. To eliminate the heat content of the products, the combustion reaction was theoretically assumed

to occur at the calorimeter-outlet temperature, approximately 400° F. The theoretical heating value of the fuel would then be the weight flow of the fuel times its lower heat of combustion at 400° F, 51,950 Btu per pound. Appendix B of reference 9 presents a detailed description of the calorimeter and heat-balance calculations used for these data. The following table shows the relative importance of the various constituents in the heat balance for a typical data point with an 80° F preheater-inlet air temperature and a total of 0.0320 pound per second of fuel at 60° F:

Constituent	Temperature change, °F	Enthalpy rise, Btu/sec
Air	80 to 400	107
Fuel	60 to 400	37
Quench water	50(l) to 400(g)	1280
Losses of calorimeter to room air, calculated	300° F (wall temperature)	20
Total		1444

The probable error in combustion efficiency from measurements of fuel, air, and quench-water flow was ±3 percent.

$$\text{Combustion efficiency} = \frac{\text{Enthalpy rise}}{\text{Fuel heating value}} = \frac{1444}{(0.0320)(51,950)} = 87 \text{ percent}$$

Pressure Loss

Afterburner fuel-injector-flameholder pressure drop or drag was measured by wall static-pressure taps with only the preheater burning to supply normal inlet conditions. The momentum heat addition pressure loss in the afterburner was measured by a series of pressure taps, with the lowest reading (farthest downstream) being used to calculate the percent pressure loss $\Delta p/p$. Total-pressure rakes were installed near the end of the program and measured total-pressure flameholder drag and momentum pressure loss for configuration G only.

Inlet Profiles

The afterburner-inlet profiles are shown in figure 4. The vertical velocity profile was calculated using the total-pressure-rake readings and the calculated preheater-outlet temperature and assuming constant static pressure across the duct. The horizontal temperature profile was read by a Chromel-Alumel thermocouple rake. The readings were corrected for radiation. Neither the velocity nor the temperature profiles thus measured were used to calculate the average inlet conditions presented later in the report, but are shown here to give the reader an idea of the profile shape and size.

RESULTS

Figure 5 and table I present combustion efficiency and pressure loss data for each of the seven individual configurations: A, swirl cans; B, spray bars; C, shielded spray bars; D, piloted spray bars; E, V-gutter; F, Pabst burners; and G, shrouded spray bars. The performance is summarized in figure 6(a) for the low-inlet-velocity condition and in figure 6(b) for the high-inlet-velocity condition.

Performance at Low-Inlet-Velocity Condition

The combustion efficiency at the low-inlet-velocity condition was approximately the same for most of the configurations, that is, about 90 percent for equivalence ratios of 0.6 to 1.0. Configurations E, F, and G, however, tended to fall off somewhat in combustion efficiency at the rich end of the curve. The preheater combustion efficiency, only about 80 percent, was represented by data points in the equivalence-ratio range of 0.25. The dashed line between the lean end of the afterburner data and the preheater point does not imply that the combustion-efficiency curve would follow the dashed line, but merely serves to connect the preheater point for identification.

The static-pressure loss or drag of the flameholders was very low, ranging from 1 to 3 percent $\Delta p/p$ for configurations A to F. Configuration E was not measured because of faulty instrumentation. Configuration G, shrouded spray bars, was designed with more burner area blockage, and the 5-percent $\Delta p/p$ loss compares with the value reported in reference 7 for this configuration. The static-pressure drop across the flameholders corresponds closely to a total-pressure drop at the afterburner-inlet velocities. The static-pressure drop resulting from heat addition, however, considerably exceeds the corresponding total-pressure drop as shown in the theoretical curves of figures 6(a) or (b). Some measured static-pressure losses were found to be lower than the theoretical values (calculated for 100-percent heat addition). Lowest losses were found for configuration A, swirl cans, which was also among the more efficient.

Performance at High-Inlet-Velocity Condition

The over-all combustion efficiency at the high-inlet-velocity condition varied from 89 to 70 percent as can be seen by the solid symbols in figures 5(a) to (g) and in the summary plot (fig. 6(b)). All the configurations tended to become less efficient as the equivalence ratio was increased. The highest combustion efficiency (89 to 85 percent) was obtained with configuration D, piloted spray bars, while the lowest efficiency was with configuration B, flattened spray bars. As expected, every configuration was less efficient than when tested at the less

severe low-inlet-velocity condition. The higher inlet velocity resulted in a shorter reaction or burner stay time. Coupled with the high velocity was a lower burner pressure which caused a slower reaction or combustion rate.

The static-pressure drop across the flameholders at the high-inlet-velocity condition was 1 to 7 percent $\Delta p/p$. The lowest measured loss was for configuration E, V-gutters, but configurations A and B, swirl cans and spray bars, also had a small flameholder pressure loss. Note that for most of the runs made with configuration G (figs. 5(g) and 6(b)) total-pressure drops were measured across both the flameholder and the combustion zone.

The measured heat-addition pressure loss for configurations A to F was equal to or less than the theoretical value for ideal or 100-percent combustion efficiency. The actual values of $\Delta p/p$ varied from 12 to 20 percent with the order of the curves being almost the same as for the combustion efficiency; that is, the less efficient combustors caused lower pressure losses. The heat-addition-loss curve for configuration G is the lowest of all, but this curve is for total-pressure loss. It should not be compared with the static-pressure curves, but rather with the theoretical total-pressure curve.

Blowout Velocity and Pressure

The afterburner would not blow out within the facility limits for inlet air temperatures of 1660° R. To obtain the blowout velocities presented, the preheater was turned off and the inlet air temperature was held at 540° R (80° F). Figure 7 is a logarithmic plot of blowout velocity against blowout pressure for configurations A, B, D, and F. A blowout point was obtained by holding the burner at a constant airflow and an equivalence ratio of 0.4. The burner pressure was then lowered until blowout was observed. Usually the burning became rough as blowout was approached, which enabled blowout to be easily noted by a sudden reduction in noise. The piloted spray bars, configuration D, had the best blowout (most stable) characteristics with configuration A being the second best.

Flameholder Durability

All the configurations were fabricated of Inconel or stainless steel, and each was operated in the course of taking data for at least 2 hours at afterburner conditions. The only burnout of any fuel-injector-flameholder occurred with configuration C, shielded spray bars. The burnout was confined to parts of the perforated side shielding in the region nearest the simulated centerbody. In this region, the inlet gas

temperatures greatly exceeded the average value (1660° R) and undoubtedly were responsible for the damage. For all seven configurations, the part of the flameholder that was in this region became heavily oxidized, which indicated metal temperatures near 3000° R. None of the other configurations, however, received any damage to the metal except for a slight warpage of the shields or ends of spray tubes. Although all the configurations would be durable at a 1660° R flat inlet temperature, spray bars, cooled by fuel passage, are far more durable than the shrouds, shields, and swirl cans. These exposed uncooled shrouds and shields are of marginal, but dependable, durability at 1660° R and will probably fail at higher inlet temperatures.

Pulsed Inlet Airflow

An attempt was made to produce a more severe operating requirement for the fuel-injector-flameholders by pulsing the inlet airflow. In addition, the pulsed airflow would partially simulate the turbulence found in a real afterburner behind a turbine. The airflow was pulsed upstream of the preheater at frequencies of 40 to 400 cycles per second by means of a rotating wheel and slot arrangement mounted in the air supply line. The static-pressure amplitude measured at an antinode in the burner varied from 0.5- to 10-percent root-mean-square $\Delta p/p$. This pressure amplitude corresponded to a velocity fluctuation at the flameholder of ±10 to ±300 feet per second. (The average afterburner-inlet velocity was 400 to 500 feet per second.) The normal combustion noise level was 1- to 5-percent root-mean-square $\Delta p/p$, the higher value occurring at higher equivalence ratios. Three configurations, A, B, and D, were tested at various inlet burner conditions and pulsed air frequencies. The pressure root-mean-square amplitude (also velocity fluctuation) was a maximum when the flow pulser was operated at the natural frequencies of the burner.

For the three configurations tested with the pulsed airflow, there was no decrease in either the over-all combustion efficiency or the burner stability in the afterburner and preheater. If any change was noticed, it was that of a slight increase in combustion efficiency at the higher resonant frequencies.

DISCUSSION

Combustion Efficiency

The combustion efficiency was reasonably high for all configurations and test conditions, thus, there is no outstanding choice on the basis of combustion efficiency alone. The configurations C, D, E, and F do not differ much in combustion efficiency with inlet conditions, and

their operating range could probably be extended beyond the inlet conditions of this report. The operational limits of the simple spray bars, configuration B, do not appear sensitive to inlet conditions until the pressure becomes lower than 12 inches of mercury absolute or the temperature lower than 1660° R. This observation agrees with the data of reference 2, which gives high combustion efficiencies at higher pressures, and reference 3, which presents lower combustion efficiencies at lower pressures for simple spray bars. Also, the combustion efficiency of configuration G, shrouded spray bars, decreases faster than would be expected from reference 7 on the basis of reduced burner pressure alone. For this configuration, quite possibly the injector shrouds were too coarse to allow complete mixing of the fuel within the burner length. The burner stay time, particularly at the high-inlet-velocity condition, was much shorter than it was at the ramjet conditions of reference 7.

The predominant cause of combustion inefficiency is probably insufficient mixing of the fuel and air. The efficiency could presumably be raised by lengthening the burner, but the same result might be achieved by refinement of the fuel-injector-flameholder or improvement of the inlet profiles. The burner length of 13 inches was short and definitely terminated by the quench-water spray. In reference 2 the quench-water-spray rate was varied at constant burner conditions with little effect in combustion efficiency, which thus indicates that the reaction was stopped by (or before) the spray. The inlet temperature profile varied considerably more than would an actual turbine-outlet profile. The temperature profile rake was located to give an average reading and did not record the extremely cold or hot spots noted by visual observation. The low-temperature areas would hamper combustion, perhaps even cause partial blowout, while the high temperatures caused the excessive oxidation of the flameholder parts.

Any unburned preheater fuel, if it did not burn to completion in the afterburner, would tend to lower the over-all (afterburner) combustion efficiency. Figure 5(g) illustrates this behavior in runs 15a, 15b, and 15c, in which the only condition that changed appreciably was the preheater combustion efficiency. The over-all afterburner combustion efficiencies are hence on the pessimistic side. For example, with a preheater combustion efficiency of 80 percent, the true or individual efficiency of the afterburner should be 5 percent higher than that measured at stoichiometric if none of the preheater fuel burns in the afterburner. Also, as the preheater fuel flow was set assuming a higher preheater combustion efficiency, the actual afterburner-inlet temperature was lower than ideal, which is another cause for lower afterburner efficiency.

Pressure Drop Losses

For the low-velocity test condition the flameholder pressure losses were very low primarily because the projected area blockage was low.

The actual values agree closely with calculated losses for sudden expansion across the flameholders. Configuration G had a higher $\Delta p/p$ because its area blockage was greater. Configuration E, if measured, would have undoubtedly had a flameholder $\Delta p/p$ loss of less than 1 percent because its area blockage was very small and its pressure loss at the high-velocity test condition was lowest of all configurations.

The pressure losses due to heat addition fall both above and below the theoretical curve calculated for ideal or 100-percent heat release. Only two configurations, C and G, fall appreciably higher than the theoretical, and both of these have a large flameholder area blockage, which adds a greater flameholder loss to the momentum heat addition loss. The remaining configurations have pressure loss values falling near or slightly below the theoretical curve. The order of the curves corresponds to the respective lower combustion efficiencies. The heat addition pressure loss data, however, cannot be too closely interpreted because of probable errors in the measurement of static pressure on a hot burner wall.

The pressure losses measured at the high-inlet-velocity condition follow much the same pattern, but at a higher level. The flameholder losses are in the same order as the configuration area blockages, and the heat-addition losses are less than theoretical because the combustion efficiency is much less than 100 percent. Some of the data spread between configurations is due to an undesired variation of inlet conditions.

Selection of Best Configuration

The reason for measuring blowout velocity data and pulsing the inlet airflow was to help select the best fuel-injector-flameholder configuration. All the configurations were grouped close together in their combustion efficiency, and most were close to their theoretical pressure losses. The three slightly better configurations, A, B, and D, were chosen for the further tests mentioned above. It was assumed that the configuration best withstanding these further tests would be the one that could be expected to have the greater extended operating region. Another question hoped to be answered was: how might these fuel-injector-flameholders perform in an actual full-size afterburner with its highly turbulent airflow? (The air pulser was mechanically limited to lower than actual turbine frequencies.)

Configurations A, B, and D were not affected by the pulsed airflow, and it could be assumed that these configurations would not be affected by the turbulence present in an actual afterburner. The blowout velocity tests, however, indicated that configuration D, piloted spray bars, was definitely superior to configuration B, plain spray bars, with configuration A, swirl cans, part way between. The results of figure 7 (blowout velocity) nevertheless may never apply in an afterburner because at

the high (1660° R) inlet air temperatures hydrogen fuel ignites spontaneously. The blowout velocity data might indicate a trend that, should combustion or stability ever become marginal, configuration D should be the most stable with configuration A next, and configuration B last.

If an afterburner were to be operated at the low-inlet-velocity condition, the first choice of a fuel-injector-flameholder would be between configuration A or D. Configuration A, swirl cans, is slightly lower in combustion efficiency at high equivalence ratios, but is slightly higher at the low equivalence ratios than is configuration D, piloted spray bars. An advantage for configuration A is definitely shown in the pressure loss curves where configuration A is a full 2 percent lower at all equivalence ratios. Configuration B, plain spray bars, would be the third choice.

At the high-inlet-air-velocity condition, the choice of configurations is a little more definite. Configuration D is the best choice because of its higher combustion efficiency curve. A second choice would be between configuration C with good combustion efficiency but high pressure losses or configuration F or A with less combustion efficiency but lower pressure losses. The plain spray bars, configuration B, have dropped too much lower in combustion efficiency to be competitive at the high-inlet-velocity condition.

SUMMARY OF RESULTS

Seven gaseous-hydrogen fuel-injector-flameholders were tested at a low- and a high-inlet-air-velocity condition. The nominal inlet values were: (1) velocity, 400 feet per second; pressure, 12 inches of mercury absolute; and temperature, 1660° R; (2) velocity, 500 feet per second; pressure, 10 inches of mercury absolute; and temperature, 1660° R. The following results were obtained:

1. The combustion efficiency at the lower inlet velocity condition was approximately the same for all seven burner configurations, that is, about 90 percent, but dropping slightly at stoichiometric. The better configurations were configurations A, B, and D.

2. The flameholder static-pressure loss at the lower inlet velocity condition was good (1 to 5 percent) for all seven configurations. The better configurations were A and B. The momentum static-pressure losses of configurations A and F were the lowest of the group, 6 to 10 percent.

3. The combustion efficiency at the higher inlet velocity condition varied from 89 to 70 percent for the seven configurations with configuration D, piloted spray bars, having the highest combustion efficiency.

4. The flameholder static-pressure loss at the higher inlet velocity condition was good (1 to 3 percent) for configurations E, B, and A and poor (5 to 7 percent) for the remaining configurations.

5. The three better configurations, swirl cans, spray bars, and piloted spray bars (A, B, and D), were subjected to a pulsed airflow of 40 to 400 cycles per second with no resulting change in the combustion efficiency or stability.

6. Blowout velocities at ambient inlet air temperatures showed configuration D, piloted spray bars, to be more stable than the swirl-can or spray-bar configurations.

Lewis Research Center
National Aeronautics and Space Administration
Cleveland, Ohio, December 4, 1958

REFERENCES

1. Silverstein, Abe, and Hall, Eldon W.: Liquid Hydrogen as a Jet Fuel for High-Altitude Aircraft. NACA RM E55C28a, 1955.

2. Kerslake, W. R., and Dangle, E. E.: Tests with Hydrogen Fuel in a Simulated Afterburner. NACA RM E56D13a, 1956.

3. Groesbeck, Donald E., Prince, William R., and Ciepluch, Carl C.: Evaluation of Hydrogen Fuel in a Full-Scale Afterburner. NACA RM E57H06, 1957.

4. Dangle, E. E., and Kerslake, William R.: Experimental Evaluation of Gaseous Hydrogen Fuel in a 16-Inch-Diameter Ram-Jet Engine. NACA RM E55J18, 1955.

5. Krull, H. George, and Burley, Richard R.: Effect of Burner Design Variables on Performance of 16-Inch-Diameter Ram-Jet Combustor Using Gaseous-Hydrogen Fuel. NACA RM E56J08, 1957.

6. Blackshear, Perry L., Rayle, Warren D., and Tower, Leonard K.: Experimental Determination of Gas Motion Accompanying Screeching Combustion in a 6-Inch Simulated Afterburner. NACA RM E53I28, 1953.

7. Kerslake, William R.: Combustion of Gaseous Hydrogen at Low Pressures in a 35° Sector of a 28-Inch-Diameter Ramjet Combustor. NACA RM E58A21a, 1958.

8. Rayle, Warren D., Jones, Robert E., and Friedman, Robert: Experimental Evaluation of "Swirl-Can" Elements for Hydrogen-Fuel Combustor. NACA RM E57C18, 1957.

9. Sheldon, John W.: Combustion of Gaseous Hydrogen in a Small Rectangular Ramjet Combustor. NACA RM E58D15a, 1958.

10. Pabst: Preliminary Report on the F. W. Heating Nozzle, Tested in the A-9 Wind Tunnel at L. F. A. Brunswick. Rep. No. L.F. 99, Volkenrode Trans., British M.O.S.

TABLE I. - COMBUSTION DATA OF HYDROGEN FUEL IN AN ANNULAR SECTOR

OF A 28-INCH-DIAMETER AFTERBURNER

Burner configuration	Run number	Over-all equivalence ratio	Combustion efficiency, percent	Static-pressure drop, $\Delta p/p$, percent	Afterburner-inlet conditions			
					Airflow, lb/sec	Temperature, $^{\circ}R$	Pressure, in. Hg abs	Velocity, ft/sec
A	1	[a]0.199	[a]81.1	[b]1.5	1.38	1470	13.2	326
		.561	91.3	6.5	1.38	1450	12.7	335
		.591	93.9	6.9	1.38	1520	12.7	351
		.597	88.6	6.7	1.36	1550	12.7	352
		.715	91.8	7.7	1.38	1470	12.9	335
		.779	91.6	10.4	1.38	1680	12.1	408
		.844	89.3	8.8	1.38	1510	12.7	349
		.849	91.6	8.7	1.36	1580	12.6	361
		.869	88.6	9.3	1.38	1670	12.7	385
		.968	84.7	8.8	1.38	1510	12.9	342
		.974	89.9	9.7	1.34	1580	12.5	358
		1.027	88.2	10.0	1.38	1670	12.8	384
		1.058	90.9	10.8	1.34	1580	12.2	371
A	2	[a]0.230	[a]72.9	[b]3.1	1.37	1500	9.7	452
		.625	89.5	13.3	1.36	1450	9.1	462
		.628	88.5	13.2	1.38	1470	9.0	478
		.772	84.4	15.1	1.41	1440	9.4	460
		.774	82.9	13.5	1.38	1460	9.1	468
		.876	80.6	13.9	1.38	1470	9.4	461
		.888	82.7	14.6	1.40	1440	9.7	445
		1.013	77.0	14.6	1.40	1440	10.0	429
		1.022	74.8	12.8	1.38	1470	9.8	442
B	3	[a]0.249	[a]79.8	[b]0.9	1.43	1660	12.6	401
		.780	89.3	9.6	1.40	1710	12.7	402
		.900	90.0	10.3	1.40	1690	13.2	382
		1.008	89.4	12.4	1.41	1680	12.6	399
B	4	[a]0.218	[a]80.5	[b]1.8	1.40	1550	12.4	369
		.619	86.7	8.4	1.40	1590	12.2	388
		.626	89.6	9.6	1.40	1600	12.4	385
		.658	87.1	8.2	1.42	1400	12.0	351
		.772	84.6	9.4	1.42	1400	11.7	361
		.793	86.5	8.0	1.40	1580	12.5	376
		.910	79.5	9.3	1.40	1580	12.3	380
		.984	72.8	12.3	1.42	1400	10.7	392
		1.008	78.3	10.7	1.42	1390	12.2	345
		1.018	74.1	7.6	1.40	1600	12.4	385
B	5	[a]0.228	[a]67.8	[b]1.5	1.37	1430	9.4	445
		.645	83.7	12.2	1.38	1525	9.1	491
		.779	75.5	12.0	1.38	1500	9.0	491
		.871	76.8	11.1	1.38	1460	9.4	458
		1.018	70.2	12.0	1.38	1460	8.4	513

[a]Preheater fuel only.

[b]Afterburner flameholder pressure loss.

TABLE I. - Continued. COMBUSTION DATA OF HYDROGEN FUEL IN AN ANNULAR SECTOR OF A 28-INCH-DIAMETER AFTERBURNER

Burner configuration	Run number	Over-all equivalence ratio	Combustion efficiency, percent	Static-pressure drop, $\Delta p/p$, percent	Afterburner-inlet conditions			
					Airflow, lb/sec	Temperature, $^{\circ}R$	Pressure, in. Hg abs	Velocity, ft/sec
C	6	[a]0.236	[a]74.5	[b]2.5	1.41	1540	13.0	356
		.590	85.4	9.3	1.41	1540	12.9	359
		.760	91.2	11.0	1.41	1550	12.6	370
		.853	92.0	13.2	1.41	1480	12.5	354
		.993	88.0	14.6	1.41	1520	12.6	363
C	7	[a]0.325	[a]73.8	[b]5.7	1.39	1860	9.3	591
		.615	87.6	14.7	1.41	1580	9.3	508
		.813	85.9	18.3	1.39	1740	9.7	532
		.946	83.9	20.2	1.39	1740	9.6	539
		1.059	81.6	20.4	1.39	1730	10.1	508
D	8	[a]0.270	[a]79.4	[b]2.4	1.41	1740	11.7	445
		.603	87.3	7.1	1.41	1630	13.0	374
		.781	91.9	9.7	1.41	1630	12.7	383
		.924	90.8	11.6	1.41	1640	12.5	393
		1.004	89.9	11.8	1.41	1630	12.5	390
D	9	[a]0.311	[a]72.5	[b]4.9	1.41	1790	9.5	565
		.625	87.6	15.5	1.41	1590	9.2	519
		.806	87.6	16.5	1.41	1640	9.9	495
		.923	88.5	17.6	1.41	1670	10.1	495
		1.034	84.4	19.1	1.41	1650	10.2	484
E	10	0.585	87.2	6.3	1.40	1350	11.8	338
		.725	89.1	7.8	1.38	1340	12.3	319
		.851	88.0	10.0	1.38	1330	12.1	323
		.988	85.3	12.9	1.38	1320	11.6	334
E	11	0.620	88.7	8.1	1.10	1500	9.3	378
		.785	85.9	11.0	1.10	1500	8.7	403
		.965	84.3	12.6	1.10	1480	9.0	382
		1.127	78.4	14.1	1.10	1570	9.0	410
E	12	[a]0.210	[a]73.4	[b]1.2	1.40	1430	11.7	362
		.610	80.7	11.7	1.38	1380	9.0	449
		.764	82.9	14.7	1.38	1450	9.3	459
		.878	80.3	15.2	1.38	1430	9.5	439
		1.017	79.5	16.0	1.38	1430	10.2	409
F	13	[a]0.266	[a]82.2	[b]2.9	1.38	1750	12.6	406
		.648	92.5	7.7	1.38	1730	12.6	404
		.814	88.9	8.3	1.38	1780	12.6	415
		.923	85.0	9.7	1.38	1770	12.3	421
		1.052	78.1	10.3	1.38	1750	12.5	411

[a]Preheater fuel only.

[b]Afterburner flameholder pressure loss.

TABLE I. - Concluded. COMBUSTION DATA OF HYDROGEN FUEL IN AN ANNULAR SECTOR OF A 28-INCH-DIAMETER AFTERBURNER

Burner configuration	Run number	Over-all equivalence ratio	Combustion efficiency, percent	Static-pressure drop, $\Delta p/p$, percent	Afterburner-inlet conditions			
					Airflow, lb/sec	Temperature, °R	Pressure, in. Hg abs	Velocity, ft/sec
F	14	[a]0.271	[a]77.8	[b]5.2	1.38	1720	9.8	510
		.663	88.2	12.6	1.38	1690	9.8	504
		.819	84.0	13.1	1.38	1720	9.8	514
		.928	80.5	13.1	1.38	1720	9.9	510
		1.065	74.6	13.0	1.38	1710	9.9	508
G	15a	[a]0.259	[a]86.7	[b]5.2	1.40	1800	12.5	430
		.656	91.1	11.0	1.40	1800	12.6	426
		.802	90.5	13.6	1.40	1840	12.2	448
		.908	88.0	14.1	1.40	1830	12.2	446
		1.054	83.9	14.5	1.40	1820	12.2	443
G	15b	[a]0.245	[a]68.6	[b,c]3.3	1.41	1500	11.9	378
		.616	88.0	[c]6.5	1.40	1350	11.9	337
		.768	88.2	[c]8.0	1.40	1350	11.9	336
		.908	84.1	[c]8.2	1.40	1350	11.9	338
		.991	80.9	[c]8.8	1.40	1350	11.9	338
G	15c	[a]0.218	[a]57.2	[b,c]4.5	1.40	1280	12.8	296
		.639	86.4	[c]6.8	1.40	1300	13.0	297
		.775	85.0	[c]7.9	1.40	1260	12.8	293
		.895	81.2	[c]8.3	1.40	1280	12.7	298
		1.003	77.2	[c]8.3	1.40	1280	12.8	297
G	16	[a]0.254	[a]71.2	[b,c]6.9	1.40	1580	9.3	503
		.416	84.0	[c]7.9	1.40	1010	10.5	285
		.614	81.9	[c]10.1	1.40	1150	10.6	323
		.646	83.1	[c]10.0	1.40	1350	9.9	406
		.763	80.7	[c]9.7	1.40	1300	11.2	346
		.903	76.6	[c]10.0	1.40	1280	11.5	329
		1.010	73.4	[c]9.8	1.40	1280	11.7	325

[a]Preheater fuel only.

[b]Afterburner flameholder pressure loss.

[c]Total-pressure loss.

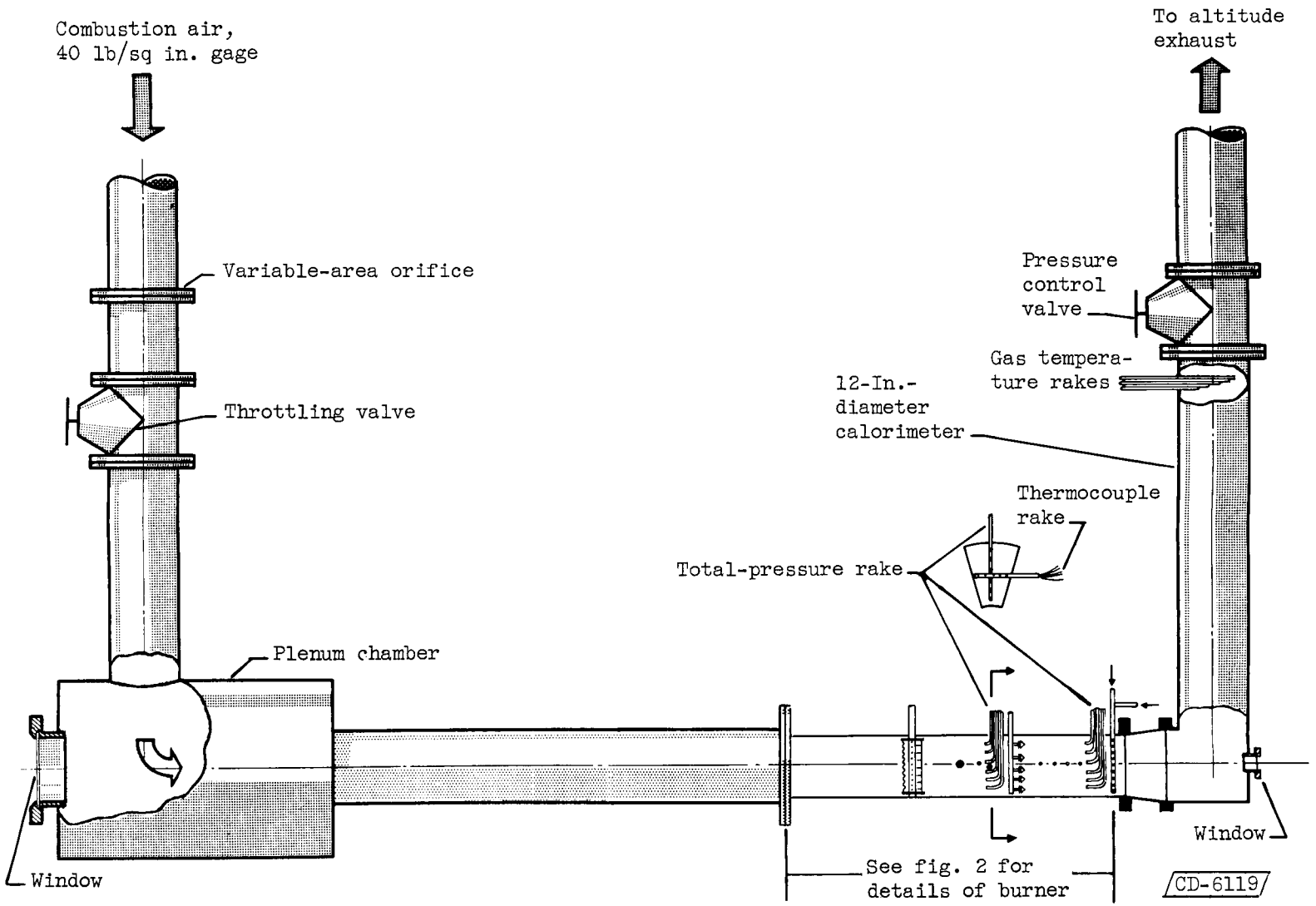

Figure 1. - Schematic diagram of installation of connection-pipe afterburner combustor.

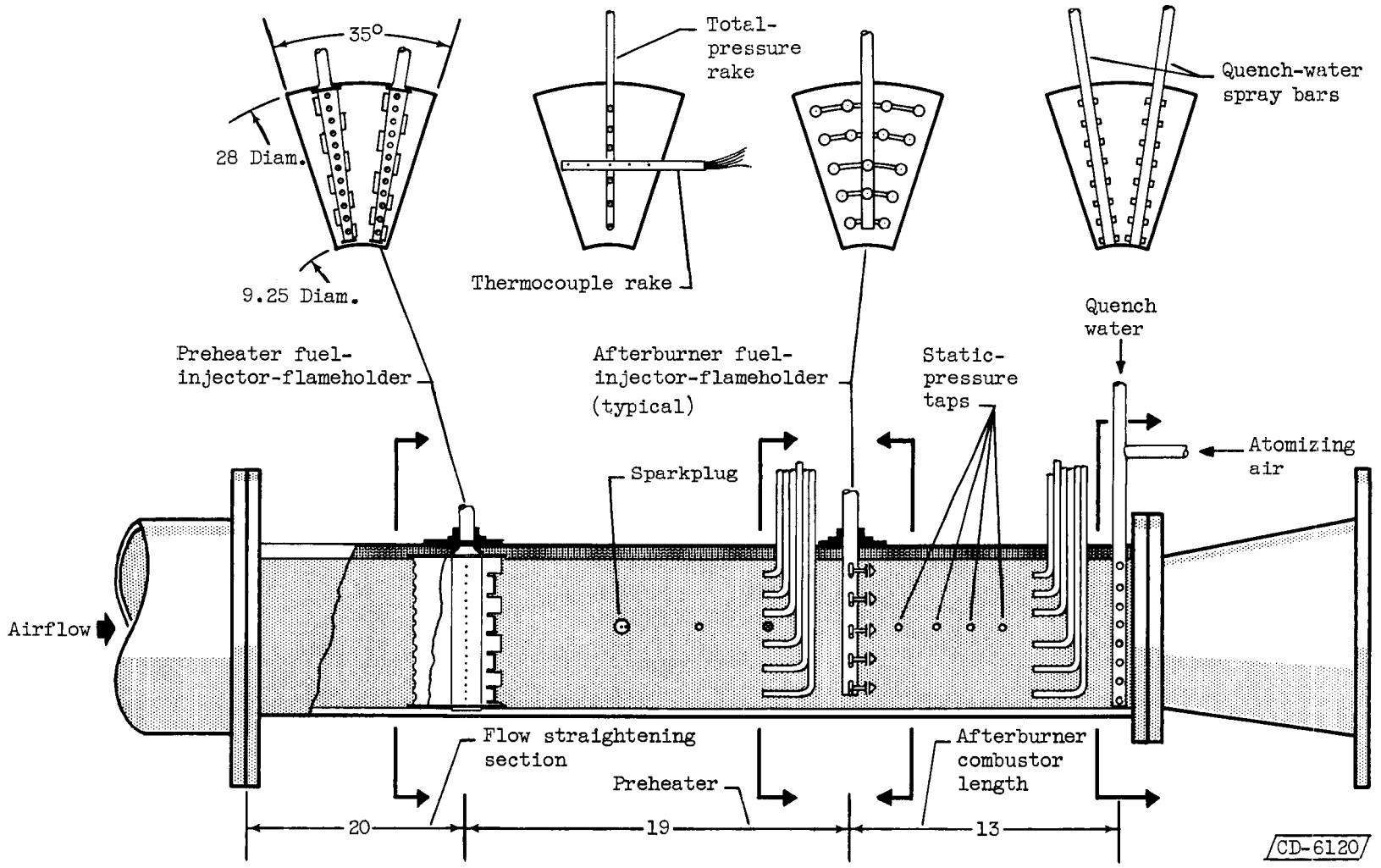

Figure 2. - Detailed view of 35° sector of a 28-inch-diameter afterburner combustor and preheater. (All dimensions in inches except where noted.)

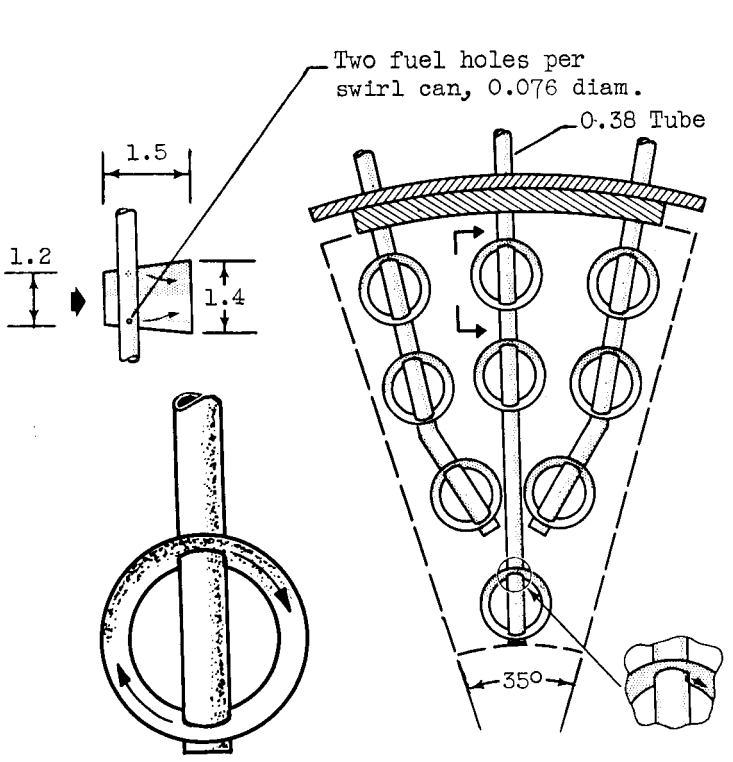

(a) Configuration A, swirl cans.

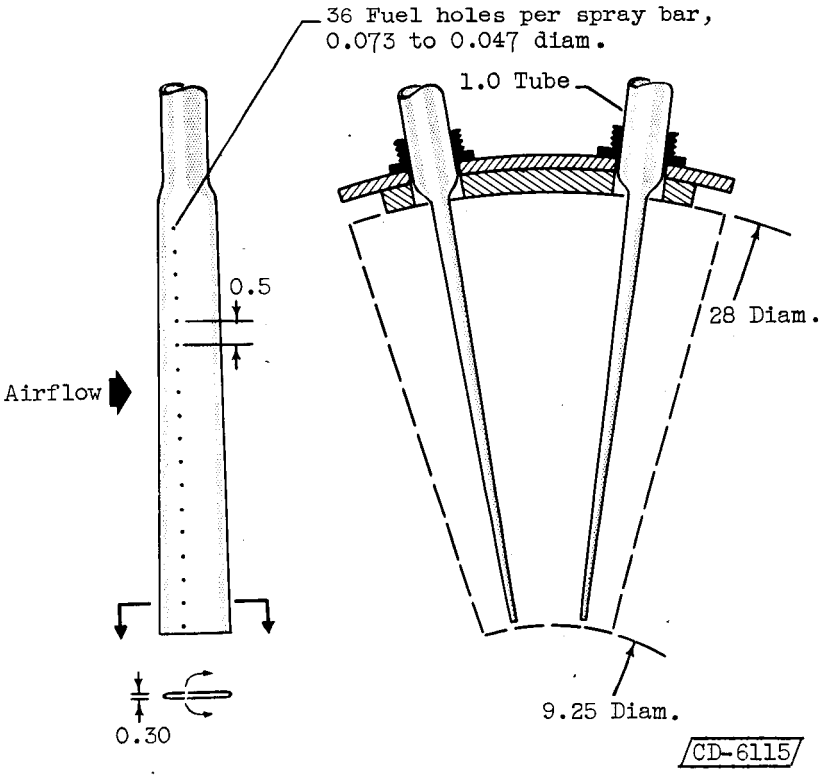

(b) Configuration B, spray bars.

Figure 3. - Details of fuel-injector-flameholders used in 35° sector of a 28-inch-diameter afterburner combustor. (All dimensions in inches except where noted.)

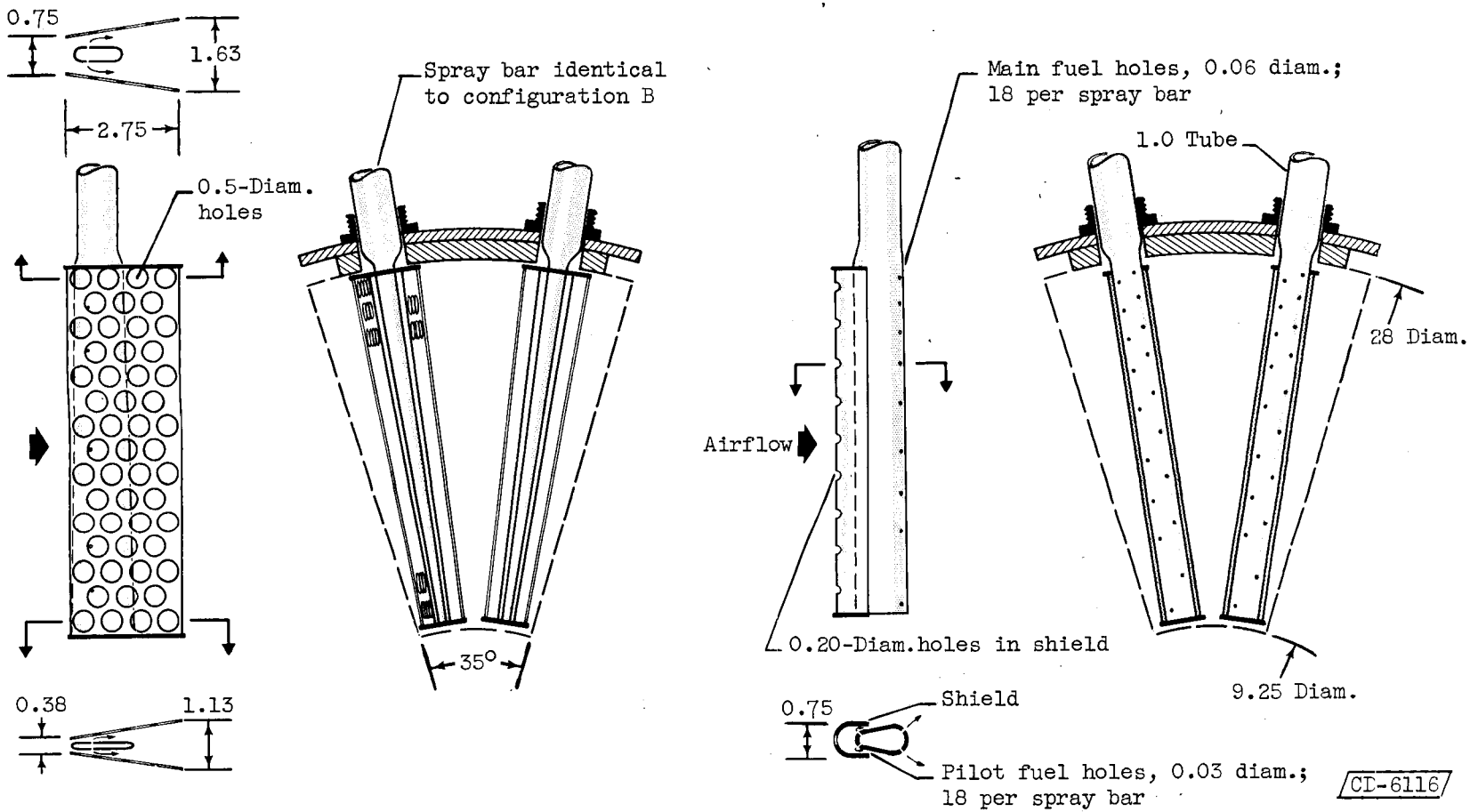

(c) Configuration C, shielded spray bars.

(d) Configuration D, piloted spray bars.

Figure 3. - Continued. Details of fuel-injector-flameholders used in 35° sector of a 28-inch-diameter afterburner combustor. (All dimensions in inches except where noted.)

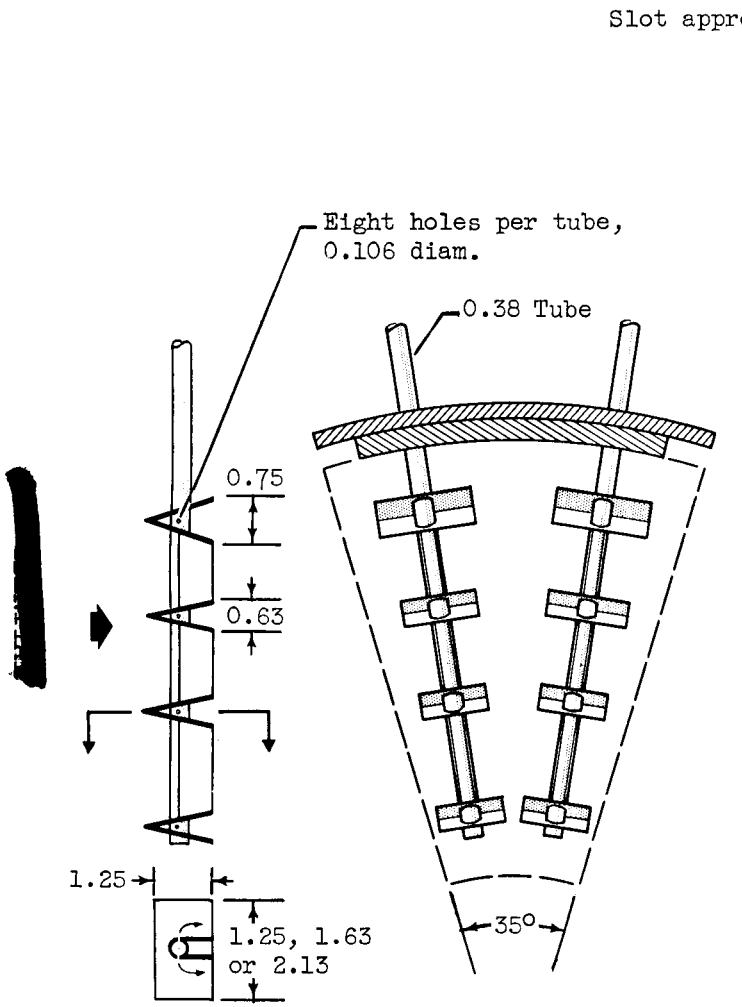

(e) Configuration E, V-gutters.

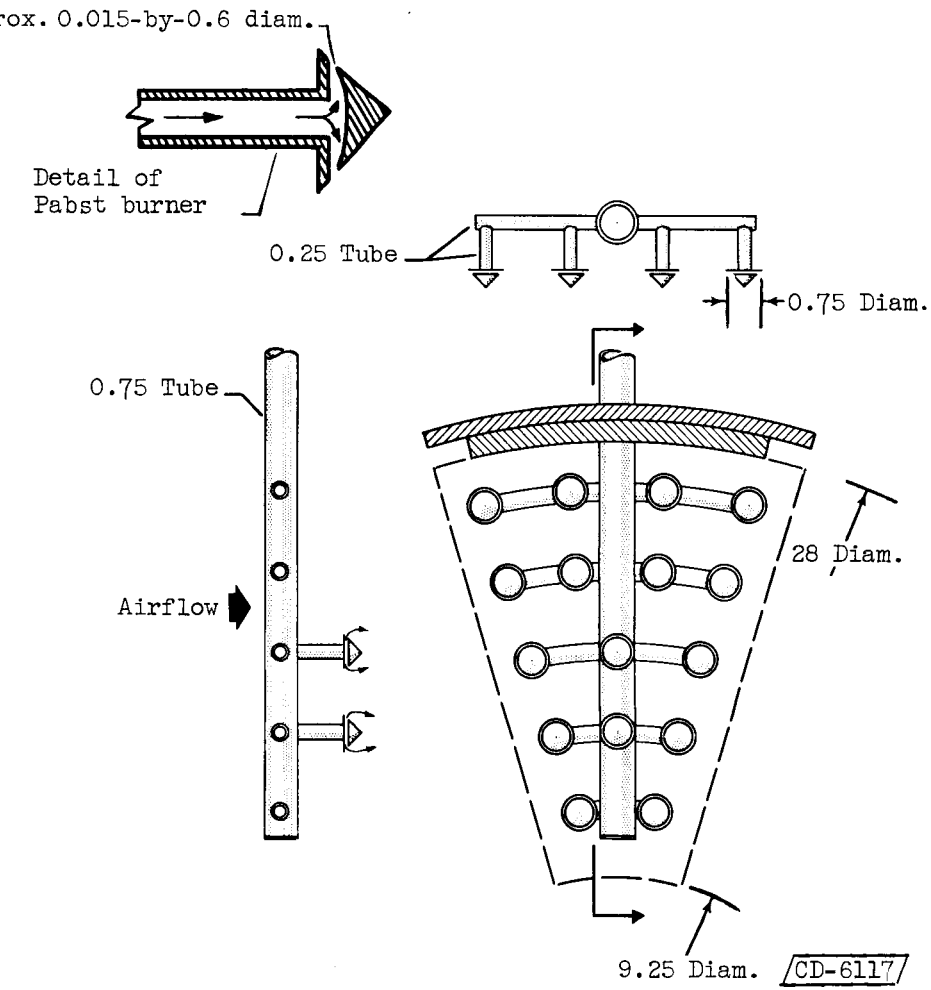

(f) Configuration F, Pabst burners.

Figure 3. - Continued. Details of fuel-injector-flameholders used in 35° sector of a 28-inch-diameter afterburner combustor. (All dimensions in inches except where noted.)

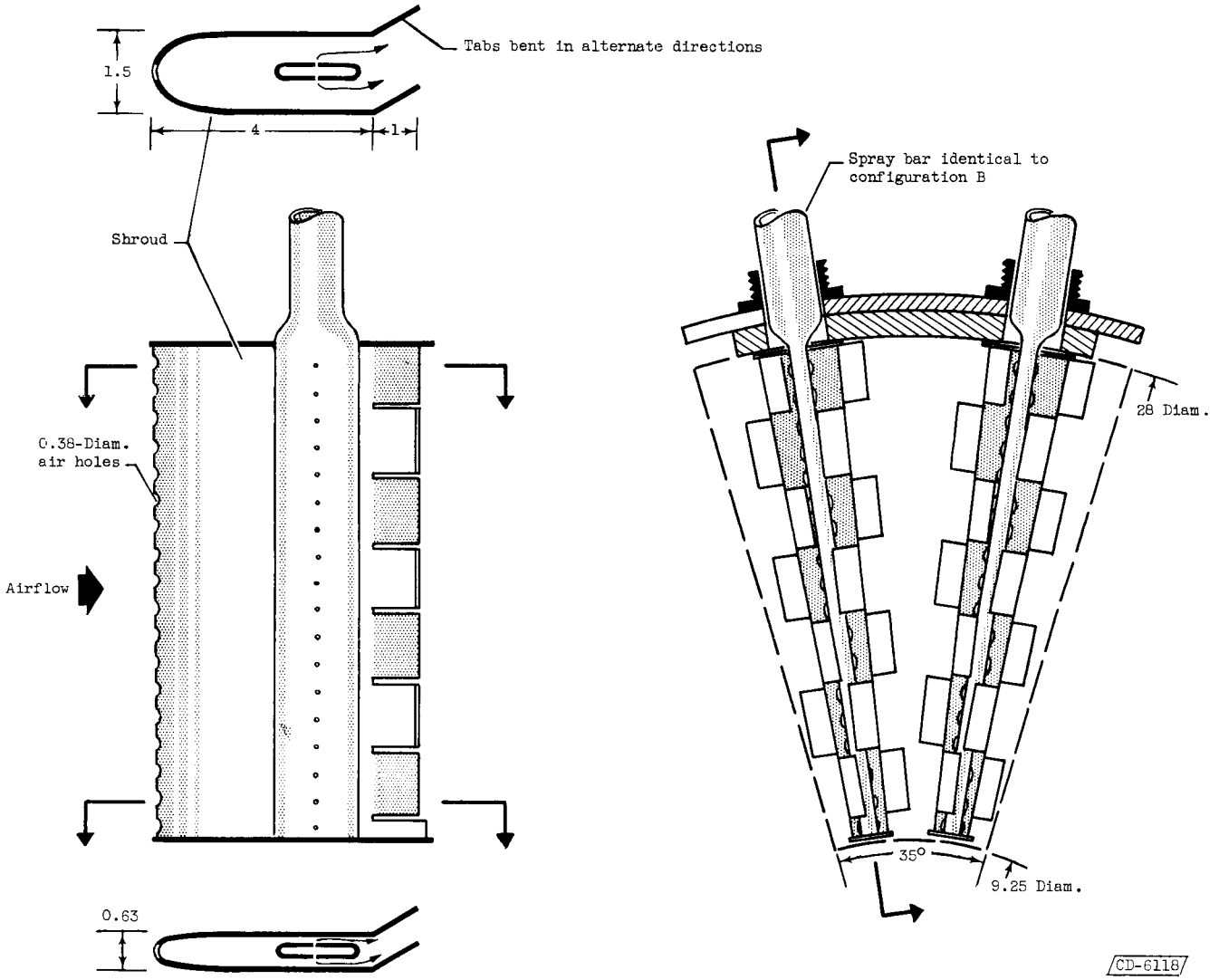

(g) Configuration G, shrouded spray bars.

Figure 3. - Concluded. Details of fuel-injector-flameholders used in 35° sector of a 28-inch-diameter afterburner combustor. (All dimensions in inches except where noted.)

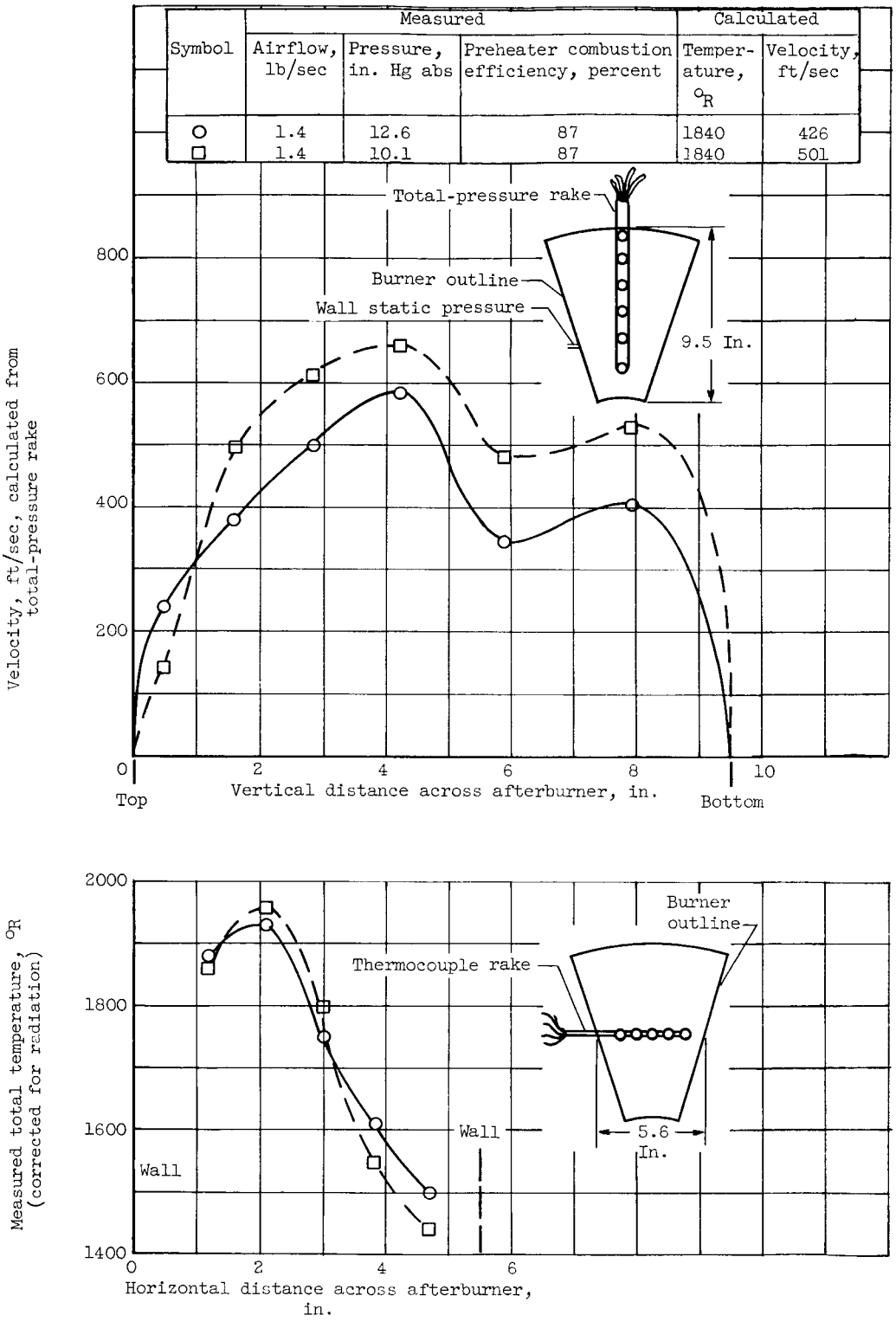

Figure 4. - Velocity and temperature profiles in a sector of a 28-inch-diameter afterburner. (See fig. 2, afterburner inlet or preheater outlet.)

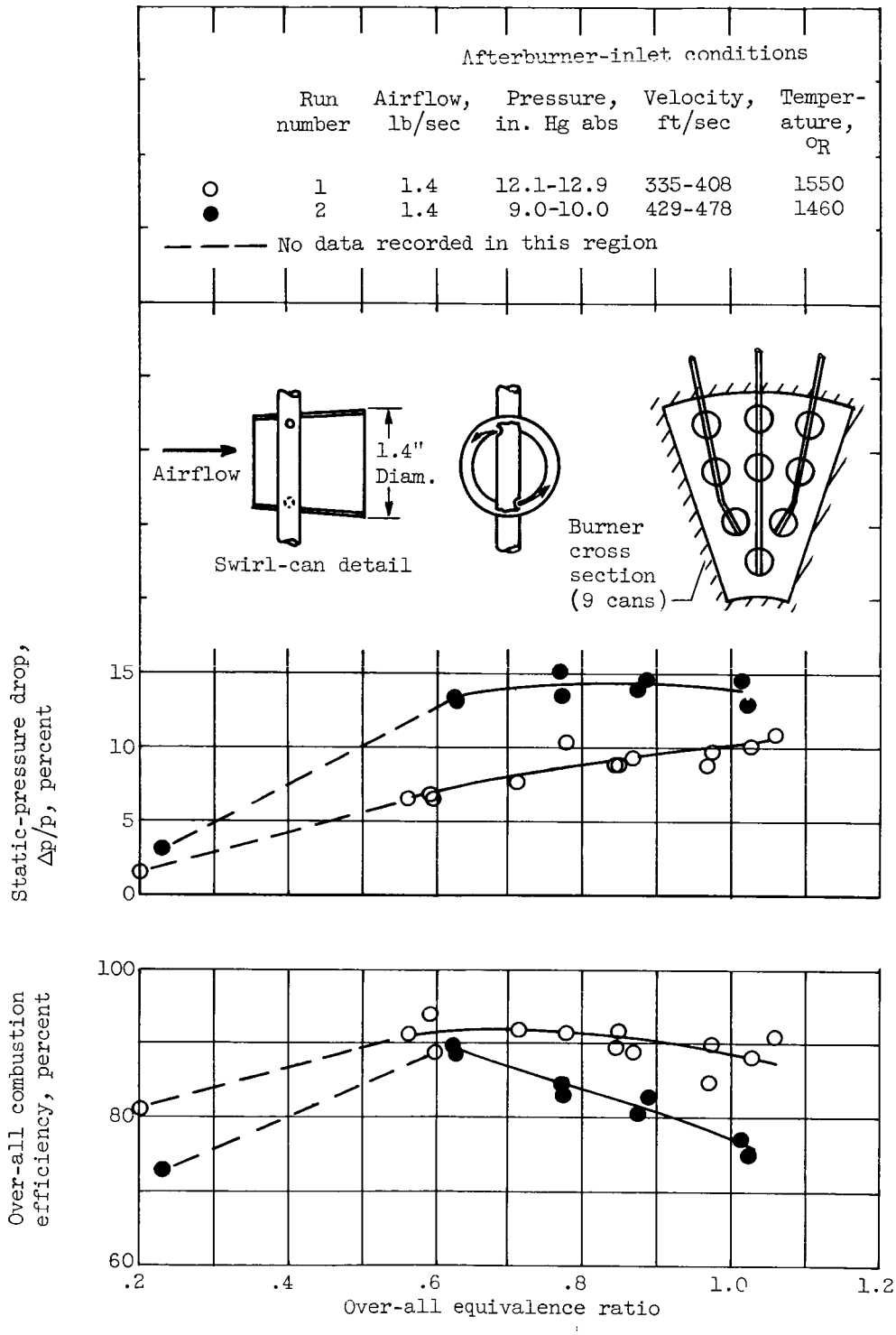

(a) Configuration A, swirl cans.

Figure 5. - Combustion efficiency of various fuel-injector-flameholder configurations in an annular sector of a 28-inch-diameter afterburner combustor. Combustor length, 13 inches.

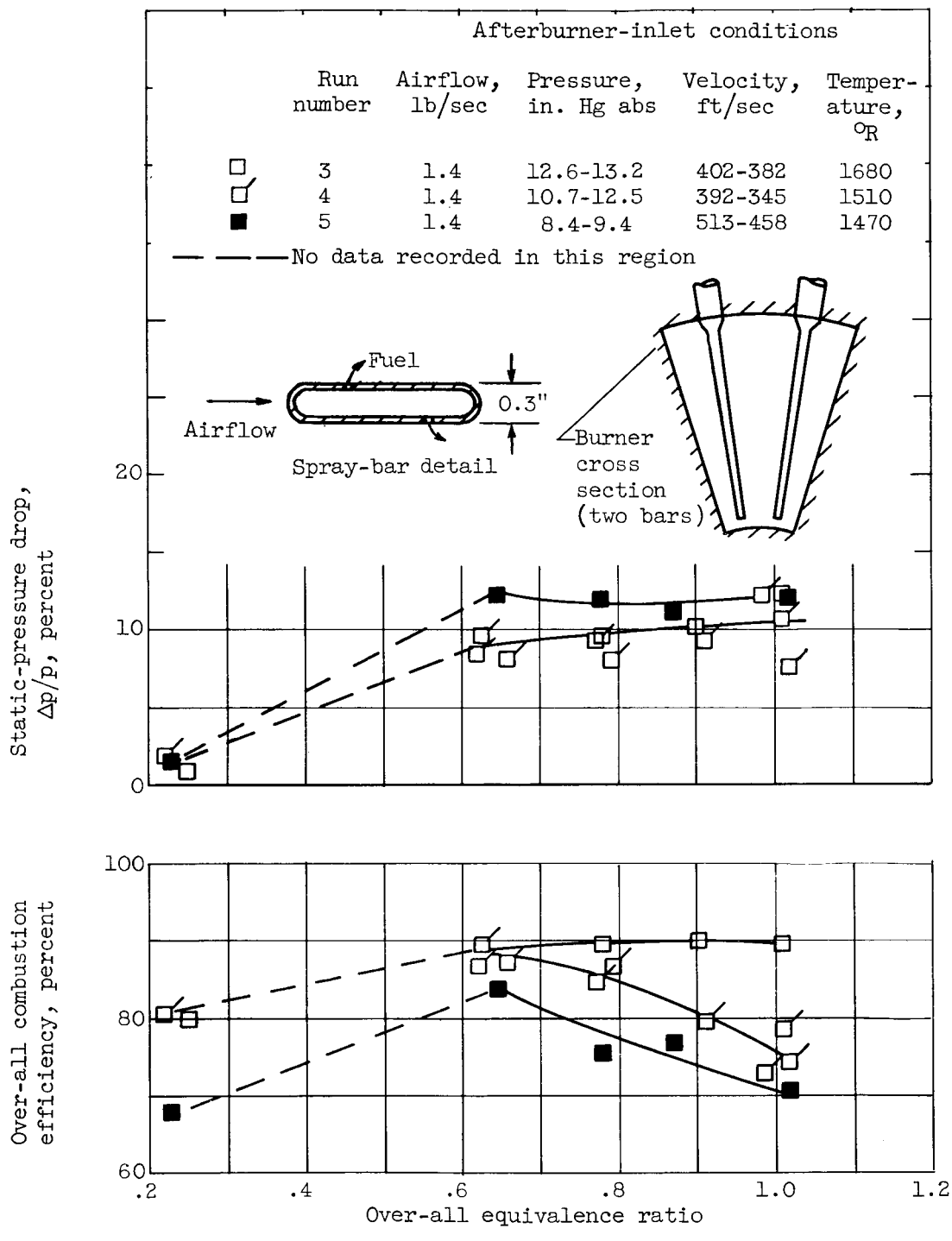

(b) Configuration B, spray bars.

Figure 5. - Continued. Combustion efficiency of various fuel-injector-flameholder configurations in an annular sector of a 28-inch-diameter afterburner combustor. Combustor length, 13 inches.

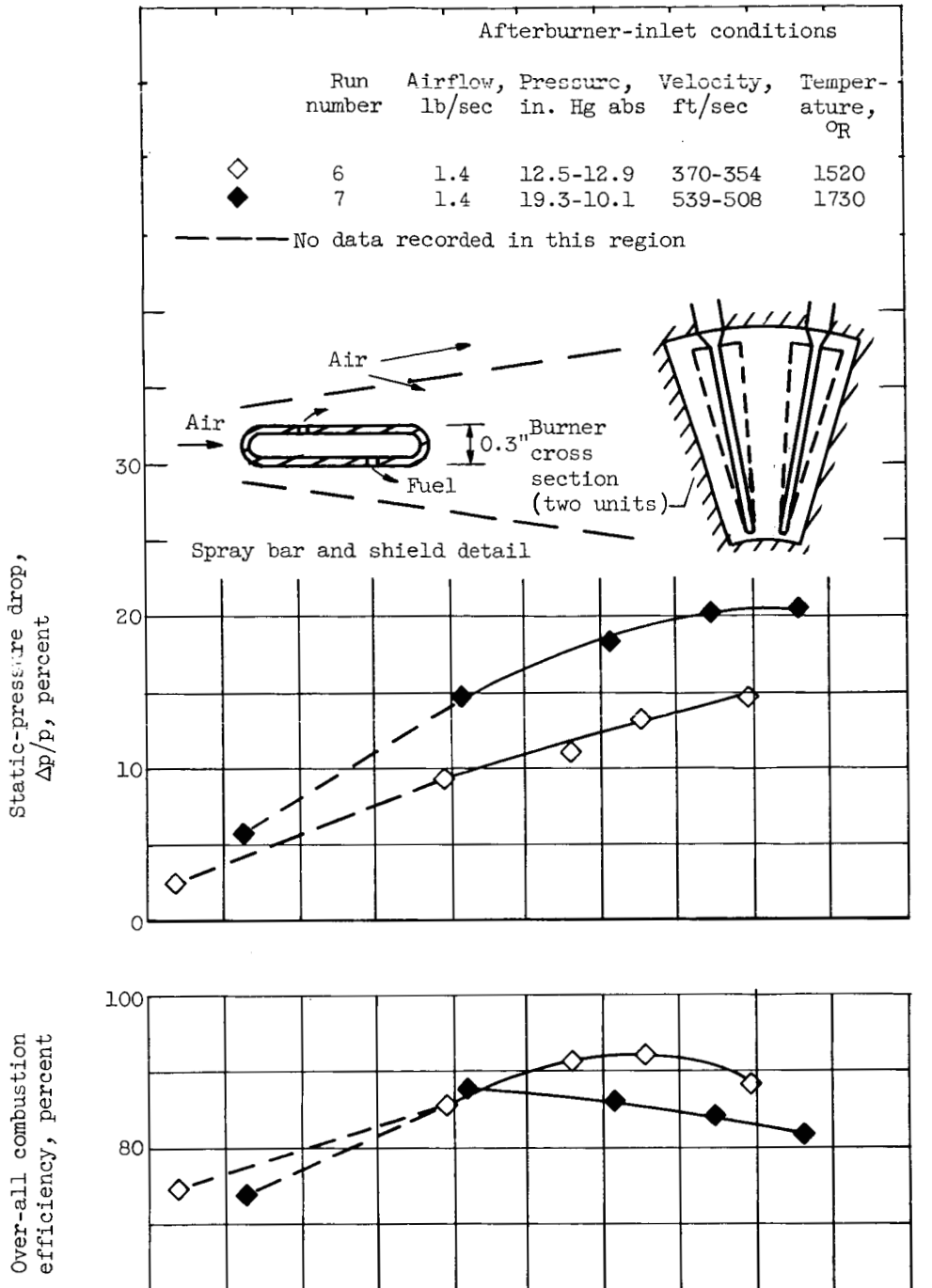

(c) Configuration C, shielded spray bars.

Figure 5. - Continued. Combustion efficiency of various fuel-injector-flameholder configurations in an annular sector of a 28-inch-diameter afterburner combustor. Combustor length, 13 inches.

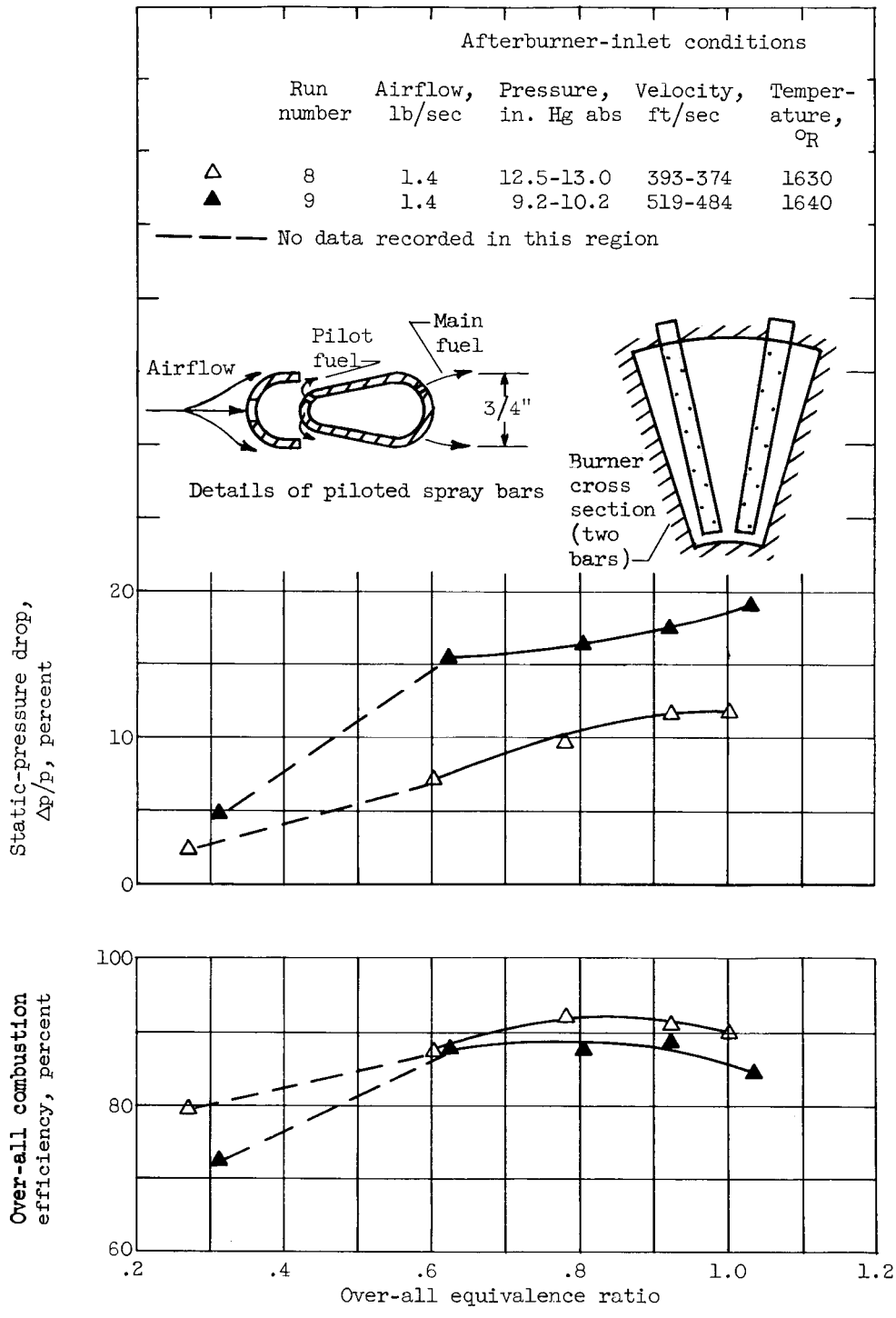

(d) Configuration D, piloted spray bars.

Figure 5. - Continued. Combustion efficiency of various fuel-injector-flameholder configurations in an annular sector of a 28-inch-diameter afterburner combustor. Combustor length, 13 inches.

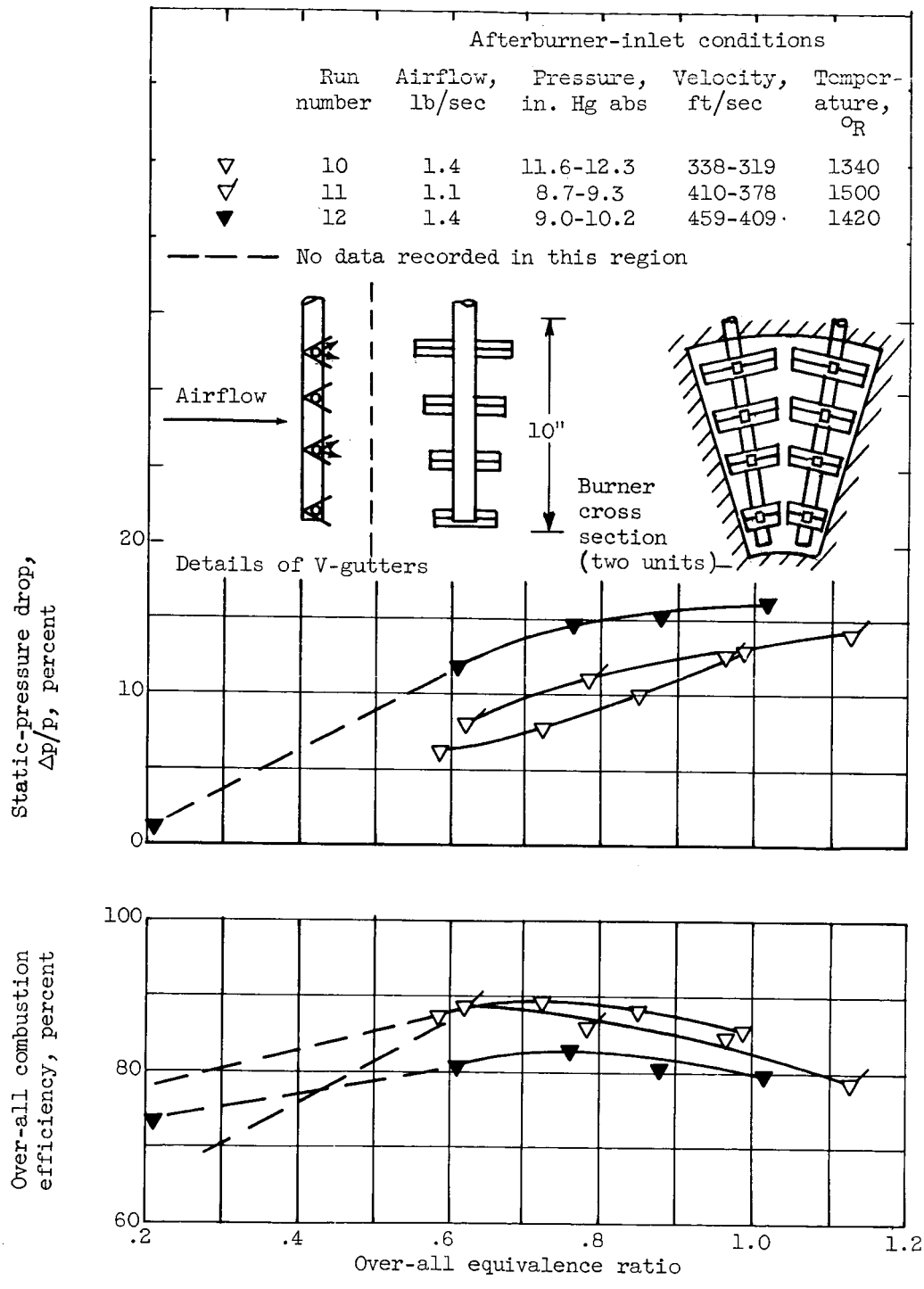

(e) Configuration E, V-gutter injectors.

Figure 5. - Continued. Combustion efficiency of various fuel-injector-flameholder configurations in an annular sector of a 28-inch-diameter afterburner combustor. Combustor length, 13 inches.

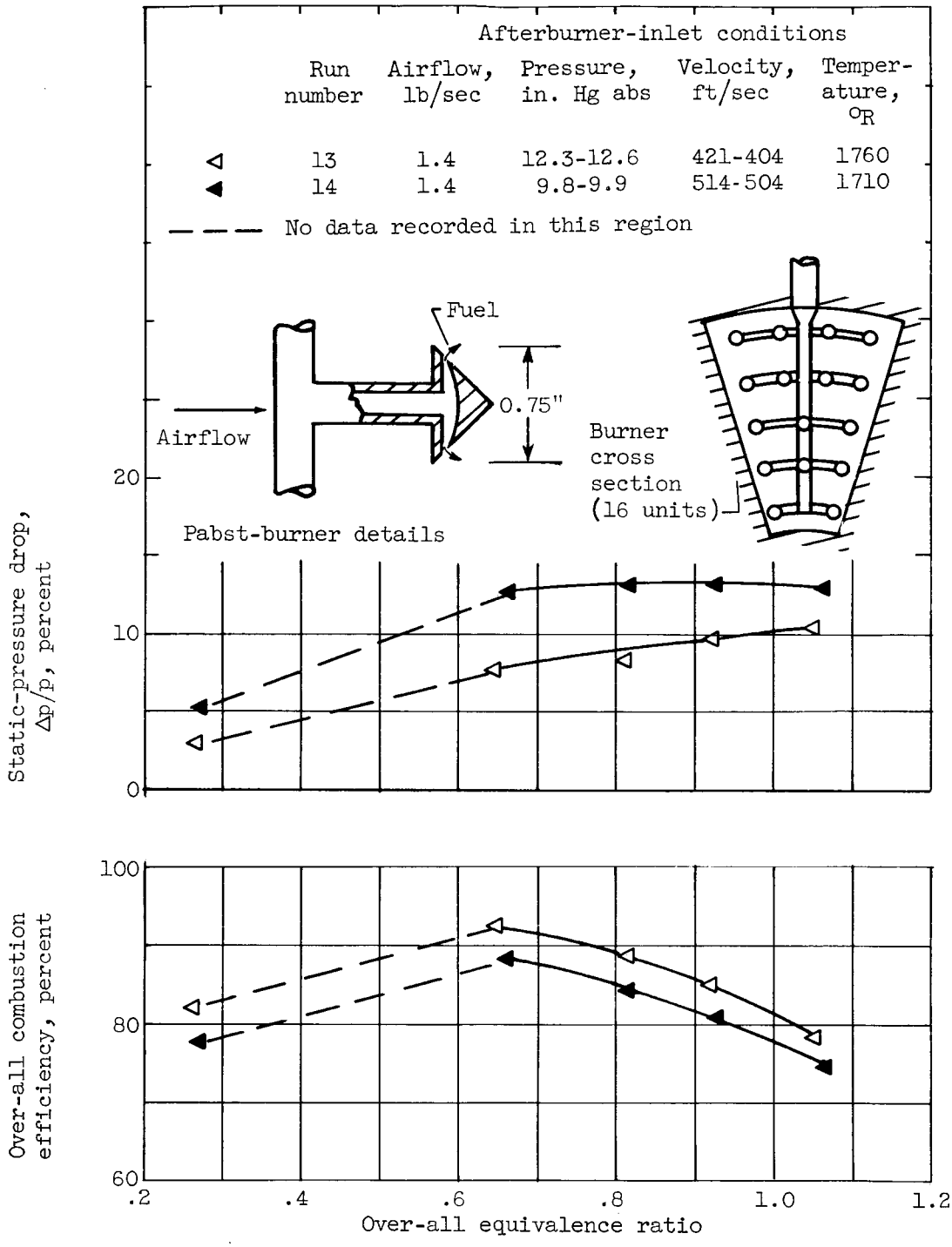

(f) Configuration F, Pabst burners.

Figure 5. - Continued. Combustion efficiency of various fuel-injector-flameholder configurations in an annular sector of a 28-inch-diameter afterburner combustor. Combustor length, 13 inches.

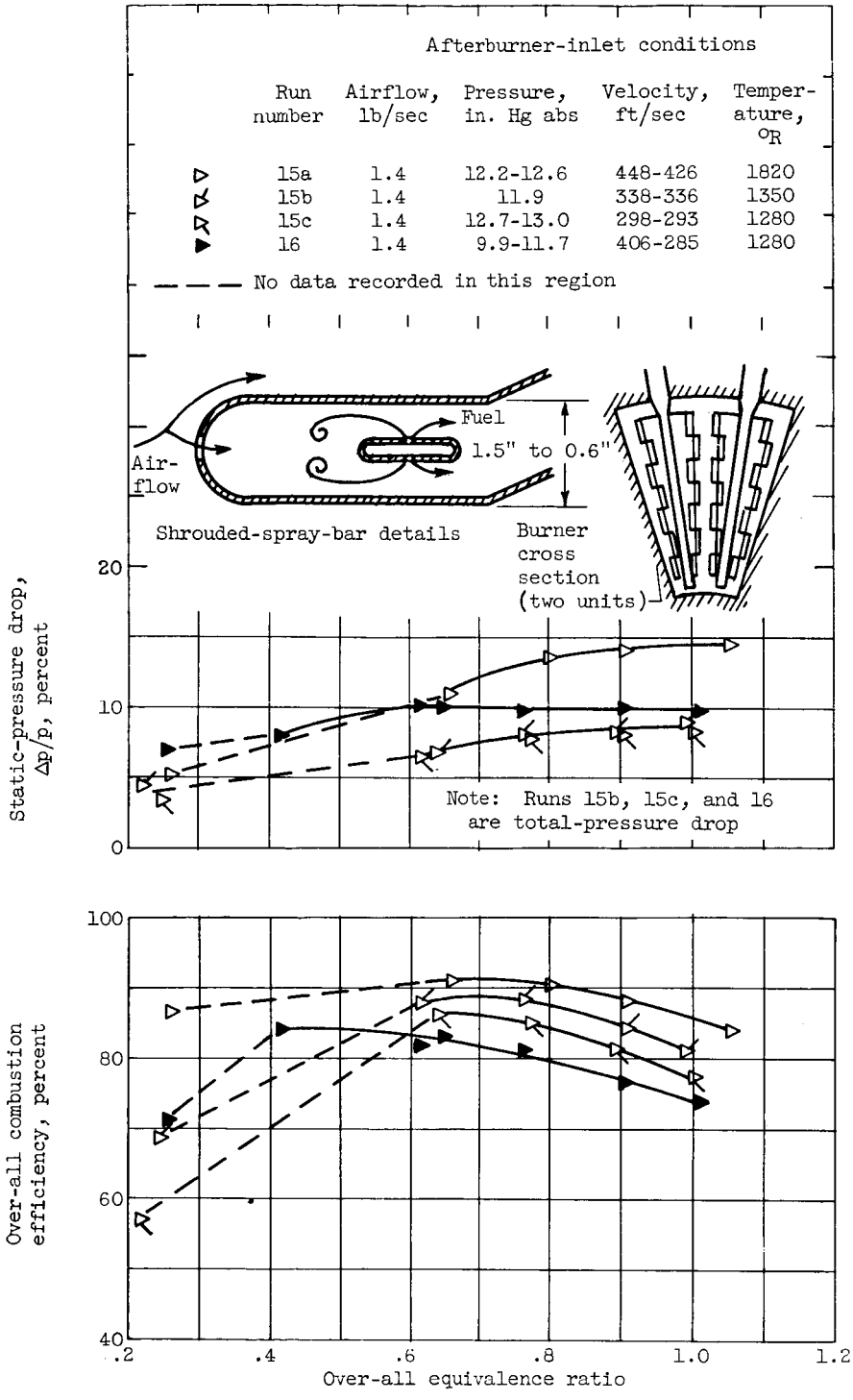

(g) Configuration G, shrouded spray bars.

Figure 5. - Concluded. Combustion efficiency of various fuel-injector-flameholder configurations in an annular sector of a 28-inch-diameter afterburner combustor. Combustor length, 13 inches.

[redacted]

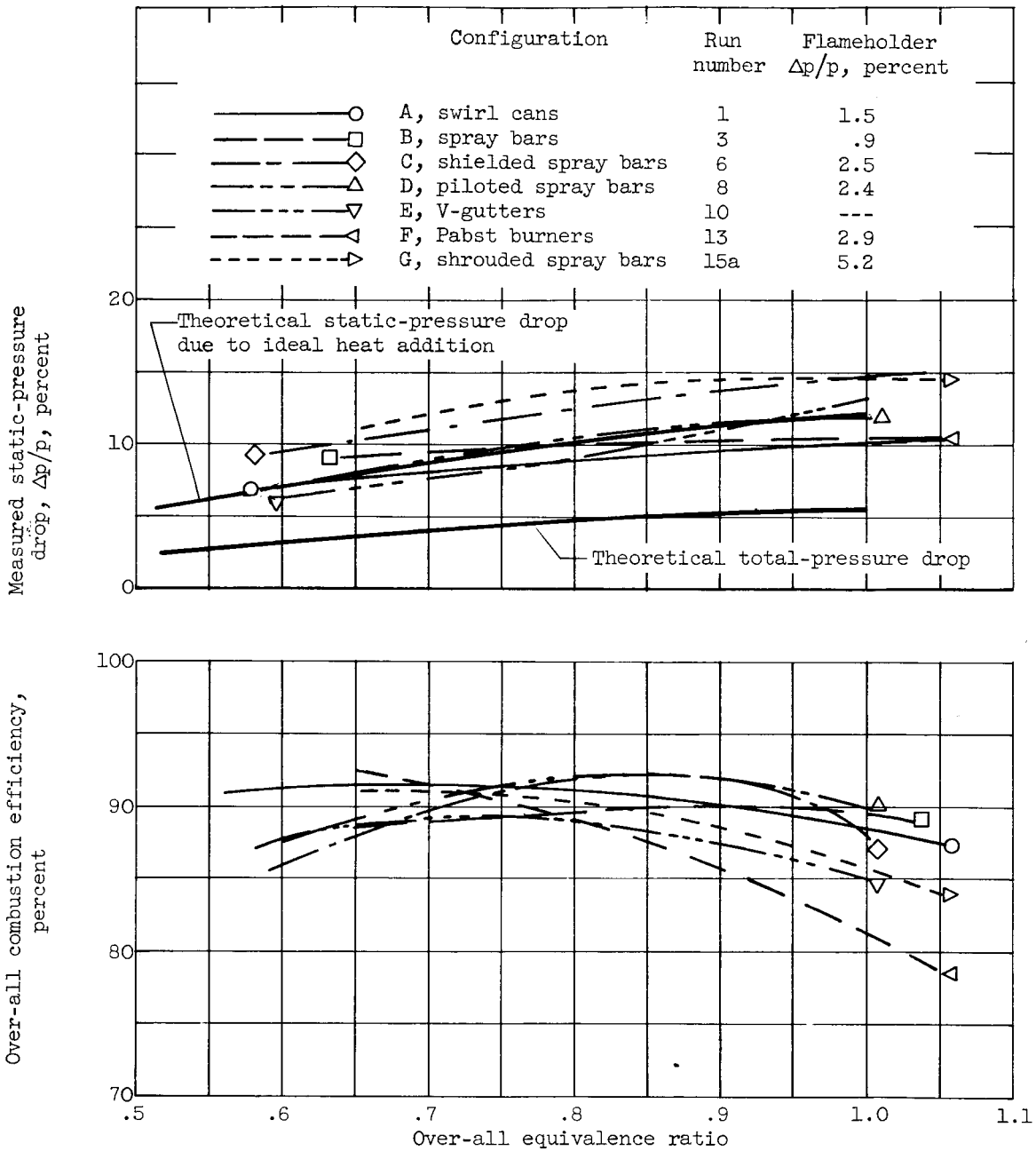

(a) Low-inlet-velocity range, nominally 400 feet per second; pressure, 12 to 13 inches of mercury absolute.

Figure 6. - Summary plot for data of configurations A to G (fig. 5). Airflow, 1.4 pounds per second; nominal inlet temperature, 1660° R. Note expanded scale on equivalence ratio and combustion efficiency.

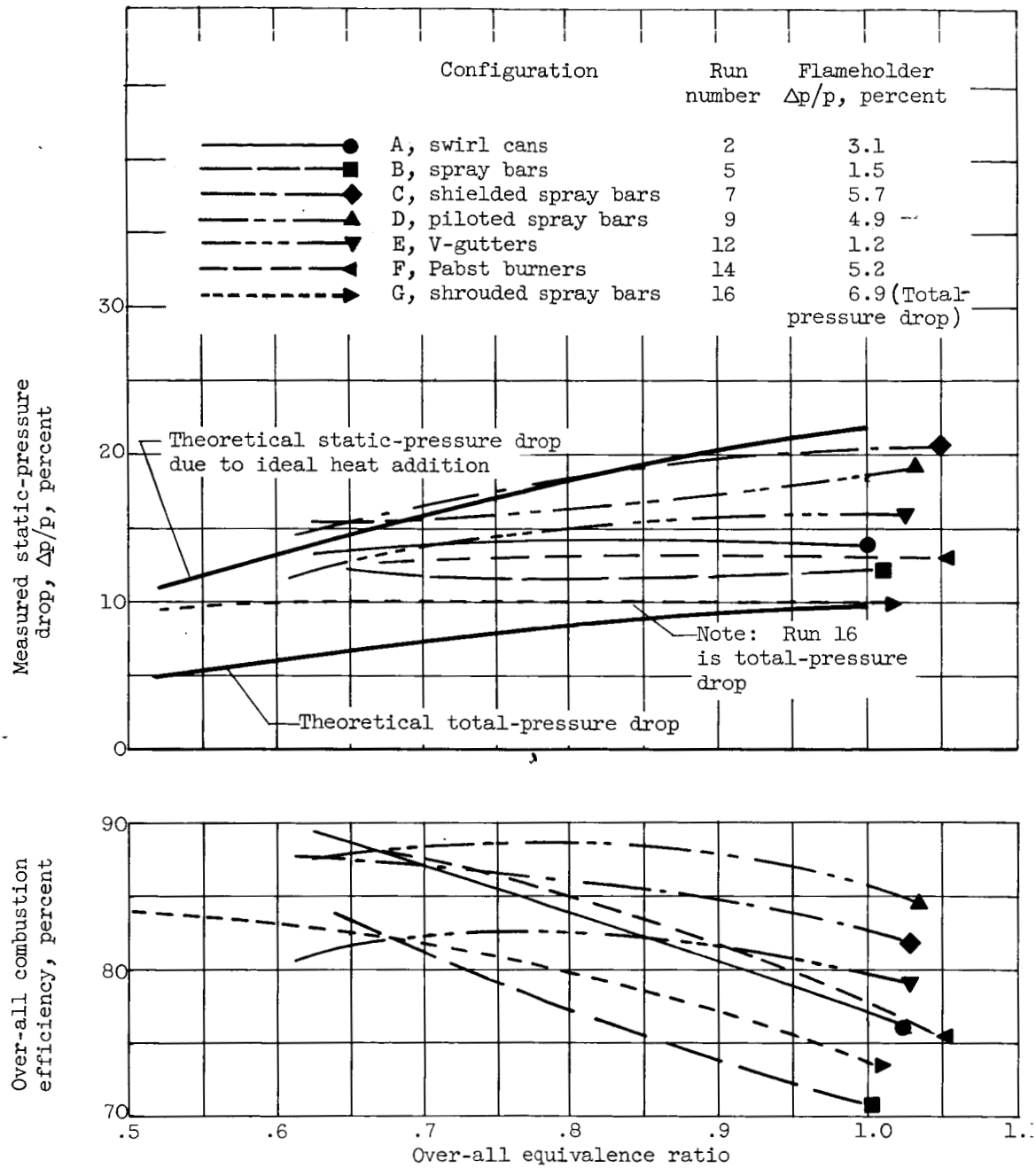

(b) High-inlet-velocity range, nominally 500 feet per second; pressure, 9 to 10 inches of mercury absolute.

Figure 6. - Concluded. Summary plot for data of configurations A to G (fig. 5). Airflow, 1.4 pounds per second; nominal inlet temperature, 1660° R. Note expanded scale on equivalence ratio and combustion efficiency.

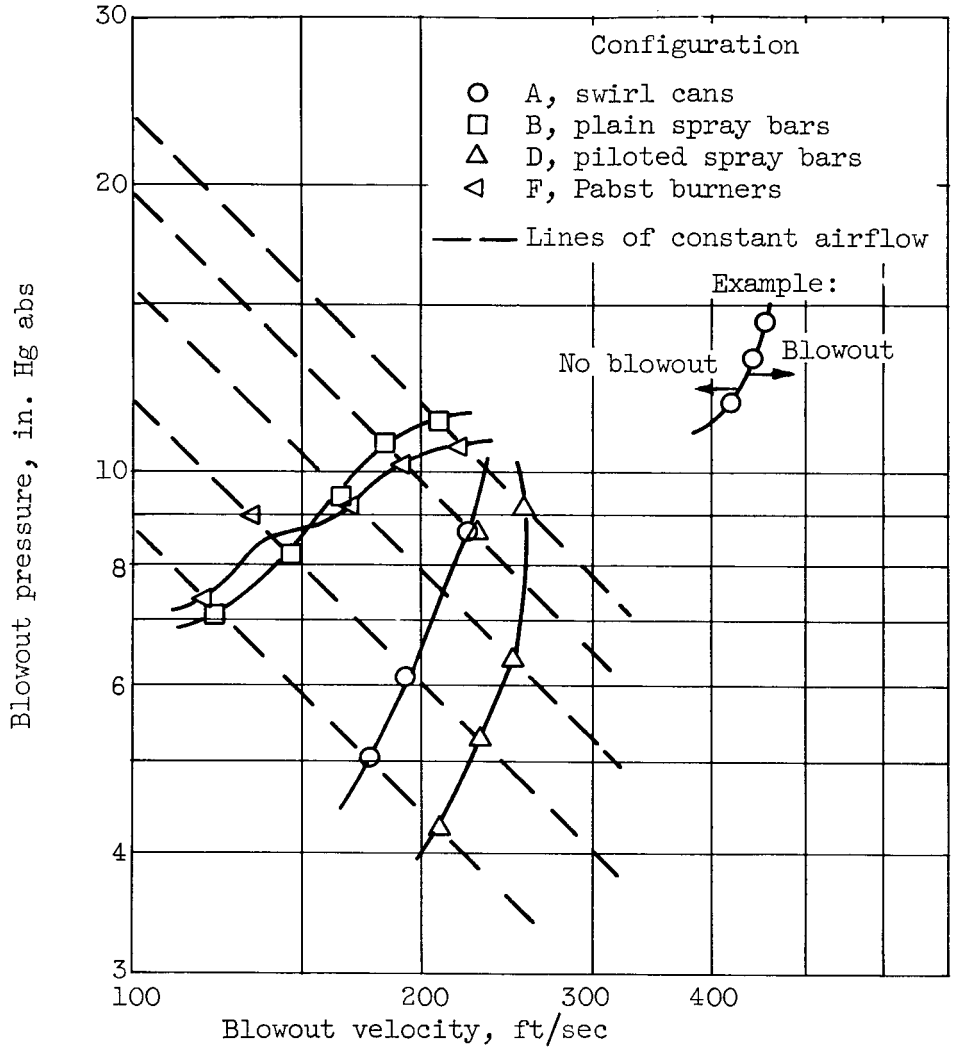

Figure 7. - Blowout limits of various fuel-injector-flameholder configurations in an annular sector of a 28-inch-diameter afterburner combustor with an inlet air temperature of 540° R. Equivalence ratio, 0.4 for all data points.